ELSEVIER

Chemical Engineering Journal 131 (2007) 23–33

Chemical Engineering Journal

www.elsevier.com/locate/cej

Multiresolution analysis of pressure fluctuations in a gas–solids fluidized bed: Application to glass beads and polyethylene powder systems

Bangyou Wu [a,b], Apostolos Kantzas [a,b,*], Céline T. Bellehumeur [b], Zhengxing He [a,b], Sergey Kryuchkov [a,b]

[a] *Tomographic Imaging and Porous Media Laboratory, Canada*

[b] *Department of Chemical and Petroleum Engineering, Schulich School of Engineering, University of Calgary, Calgary, AB, Canada T2N 1N4*

Received 4 August 2006; received in revised form 21 November 2006; accepted 2 December 2006

Abstract

Gas–solids fluidized beds are widely accepted as nonlinear and chaotic dynamic systems. Traditional methods such as statistical and spectral analyses are not sufficient to capture critical behavior in these systems. In this work, non-intrusive techniques were used to characterize the hydrodynamics in gas–solids bubbling fluidized bed using polyethylene powder and glass beads with comparable mean diameter. Pressure fluctuations and X-ray fluoroscopy measurements were performed on a pseudo two-dimensional fluidized bed. Statistical, wavelet, and chaos analyses were applied to the non-stationary pressure signal series to extract and characterize the intrinsic features of the gas–solids fluidized bed. Dominant cycle time was calculated from approximate coefficient of scale 6 decomposed from cleaned pressure fluctuation. The global bubbling behavior of the glass bead system was greatly affected by changes in the superficial gas velocity while polyethylene powder only significantly varied with the distance from the distributor. Average cycle time, dominant cycle time, Kolmogorov entropy and wavelet energy were also calculated from detail coefficients of scale 1–6 decomposed from cleaned pressure fluctuation to investigate flow dynamics at micro- and meso-scales. Similarities and difference of bubbling behavior at different scales for glass beads and polyethylene powder systems from pressure fluctuations were verified from X-ray fluoroscopy measurements. Results show that polyethylene particle systems have quite different bubble properties compared with glass beads particle systems under comparable operating conditions. The combination of statistical, chaos and wavelet analyses proved to be an effective method to characterize multi-scale flow behavior in the gas–solids fluidized bed.

Keywords: Fluidized bed; Wavelet analysis; Chaos analysis; Cycle time; Polyethylene powder

1. Introduction

Gas-phase fluidized bed reactors are used in a wide range of applications in refining, upgrading, pharmaceutical, food and chemical industry. The production of polyolefins is one important example of such applications. The modeling of the performance of fluidized bed polymerization reactors is complex and requires the consideration of mass and energy transfer at the macroscale level, intra and inter particle mass and energy transfer, particle growth, particle interactions, and kinetics of polymerization. The treatment of such system as a dense phase/dilute phase binary is probably oversimplied and ultimately, realistic hydrodynamic models are necessary for the design, scale-up, operation optimization and assessment of an existing and new polymerization processes. Systematic work has been carried out on hydrodynamics in bubbling fluidized bed using polyethylene particles in Dr. Kantzas' group at University of Calgary. Non-intrusive methods, such as pressure fluctuation, X-ray fluoroscopy, computer assisted tomography, and radioactive particle tracking were used. Bubble properties and solids phase features were extracted. However, comparison of hydrodynamics of porous particles with non-porous particles was not sufficient. Extensive experimental work has not been performed elsewhere. Most of published fluidized bed hydrodynamic models were based on experimental results for non-porous, solid particles. Are these models suitable for porous particles like polyethylene powder? Results from a multiresolution analysis of the fluid dynamic behavior of glass-beads and polyethylene powder fluidized beds may be suitable to answer this question.

* Corresponding author. Tel.: +1 403 220 8907; fax: +1 403 282 5060.
E-mail address: akantzas@ucalgary.ca (A. Kantzas).

1385-8947/$ – see front matter © 2006 Elsevier B.V. All rights reserved.
doi:10.1016/j.cej.2006.12.001

Nomenclature

A	approximate coefficients from wavelet decomposition
ACT	average cycle time (s)
CFD	computational fluid dynamics
D	detail coefficients from wavelet decomposition
DCT	dominant cycle time (s)
h	bed height from distributor (cm)
K	Kolmogorov entropy (bits/s)
P_j	power or energy of wavelet coefficient in different dyadic scales j (amplitude)
SD	standard deviation
U_g	superficial gas velocity (cm/s)
U_{mf}	minimum fluidization velocity (cm/s)
W_{jk}	discrete wavelet coefficients
$x(t)$	square integrable function

Greek letter

$\psi(t)$	mother wavelet function

Traditional Fourier method has been used extensively in analyzing signal series from fluidized bed systems for several decades. Fourier transform and inverse Fourier transform establish one-to-one relationship between the time domain and the frequency domain [1]. Fourier analysis provides good resolution in frequency domain and some intrinsic features of flow dynamics can definitely be revealed using Fourier analysis, as there exist similarities between Fourier analysis and chaos analysis [2]. Windowed Fourier analysis and short-time Fourier analysis were introduced in order to localize the position of signal series in time domain. However, the window size cannot be changed during certain Fourier transform which greatly limits the identification of features in non-stationary systems.

Signal series from fluidized beds are often nonlinear, chaotic, and non-stationary [3]. As such, Fourier spectra obtained from measured signals do not show consistency in frequency behavior over different time segments. The reliability of the analysis performed on these signals using traditional methods is thus insufficient and wavelet analysis, also referred to as multi-resolution analysis, has been proposed to take into the non-stationary features and to analyze the dynamical behavior of fluidized bed systems in more details [3–5].

With the introduction of wavelet analysis, signal can be localized in both time and frequency, and signal series can be decomposed into different scales. While it unifies statistical, spectral and fractal feature extraction methods [6], the transformation functions in wavelet analysis have distinct characteristics compared to those used in Fourier analysis: (1) irregular shape is suitable for signal with discontinuities or sharp change; (2) compact support nature allows temporal localization. These features enable analysis of non-stationary and transient short time events. Other advantages of wavelet analysis compared to Fourier and its variants can be summarized in two key points [3]. One is that wavelet transform has more clarity because the basis functions are oscillatory mathematical entities with compact support and the spectral components do not get cluttered with repeated multiples and negative frequency components. The other is that the window size may be carried out for every single spectral component without losing any information. The fine and coarse resolution components from wavelet decomposition capture the fine and coarse features in the signals, respectively [1]. Wavelet coefficients also provide a measure of the signal energy in various regions of the time-frequency plane. Also, wavelet denoising is well accepted and shows considerable promise in studying turbulent system [3]. This method allows noise to be removed in all scales without a significant distortion of the signal.

In this study, pressure fluctuation and gas–solids flow images of glass beads and polyethylene powder systems at ambient conditions were measured. This will be the first step in the assessment of hydrodynamic models for gas–solids fluidized beds. Nonlinear flow behavior was characterized from statistical and chaos analyses of pressure fluctuations. Multi-scale flow behavior was further investigated using wavelet analysis of pressure fluctuation. Bubbling behavior form pressure fluctuation was compared with those from X-ray fluoroscopy measurement. The gas–solids flow behavior of polyethylene powder system was compared with that of glass beads powder systems.

2. Experimental

The fluidized bed system consisted in a pseudo 2D column made of Plexiglas with an inner width and thickness of 22.5 cm and 5 cm, respectively, the height of the fluidization section being 150 cm. A porous plate distributor was installed on the bottom of the column, and the gas entered the column through a cone at the bottom of an approximately 15 cm long chamber. The cone was filled with small plastic spheres (diameter = 6.35 mm) and the chamber was empty to improve the gas distribution before reaching the distributor. Valves and rotameters were used to adjust and measure the gas flow rate, respectively.

Two types of particles were tested glass-beads and polyethylene powder, with the column being filled with particles to a static bed height of 40 cm. Both particle systems had the similar mean particle size (360 μm) and particle size distribution (297–420 μm), while they differed in density (2480 kg/m^3 for glass-beads and 924 kg/m^3 for polyethylene powder). It should be noted that the polyethylene resins are porous particles. The value of 924 kg/m^3 is plaque density that will be used in the voidage calculation. The particle density and particle voidage are 0.613 g/cm^3 and 0.337, respectively. Both types of particles are classified as Geldart "B". The minimum fluidization velocity (U_{mf}) was determined by measuring the bed pressure at different velocities, and was found to be 11.0 cm/s for the glass-beads and 4.3 cm/s for the polyethylene powder. Three superficial gas velocities (U_g) were tested for each type of particles.

Four pressure transducers (Schlumberger Solartron, model 8000 DPD) were connected to four column wall pressure ports located at a height h = 6, 16, 36, and 56 cm above the distributor using 0.32 cm nylon tubes. An A/D converter, a PC-LPM-16 card from National Instruments, and a personal computer were used for data acquisition. A self-developed Labview program

records voltage data and stores them into the computer hard disc. Transducers were calibrated to establish the relationship of pressure versus voltage prior to the experimental measurements. The pressure data was collected at a rate of 500 Hz for 60 s at each flow rate. The first 16384 (2^{14}) data points were used for analysis. Each operating condition was sampled 20 times. Original purpose of 20 samples was to average out the noise. Though pressure signals were denoised using wavelet methods and one representative sample is enough for wavelet analysis, parameters estimated from pressure fluctuation data were averaged from the 20 samples.

The X-ray fluoroscopy system (Fig. 1) consisted of the X-ray tube, X-ray detector, image intensifier and image acquisition computer. The X-ray tube generates continuous X-rays by energy conversion when a stream of electrons produced at the cathode collides with a target or anode. The X-ray detector receives the attenuated X-rays passing through the object to be imaged and converts the X-ray photons to electrical signals. The image intensifier enhances the electrical signals, converts them to a digital grayscale image. According to the intensity of light, the grayscale number of the image varies from 0 (black) to 255 (white). The image acquisition computer grabs the image at the rate of 30 frames per second and stores it to the hard disc. The grayscale number was correlated to bed voidage by calibration. The effective diameter of the image was some 17 cm. The size of the image was less than the width of the column. In this research, six parts of the column were imaged at each given superficial gas velocity. For each part, approximately 2 min worth of images were collected which amounted to 3600 frames.

Neighborhood averaging scheme was applied to the images to remove noise. A global threshold of grayscale number was used to determine the bubble boundary and binarize the grayscale images. MATLAB program was written to identify and track bubbles. Additional details about the experimental setup and procedure can be found in reference [7].

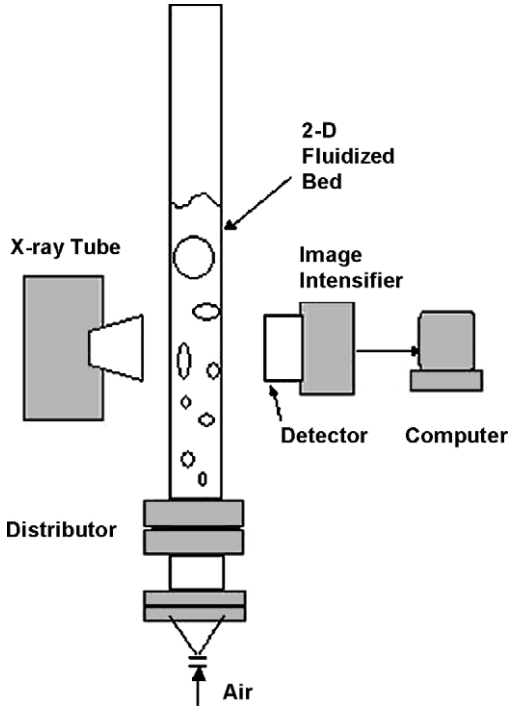

Fig. 1. Schematic of the X-ray fluoroscopy setup.

3. Methods of analysis

3.1. Wavelet analysis

Wavelets are a family of functions of constant shape and zero mean that are localized in both the frequency and time domains. Only one-dimensional wavelet transform will be covered in this section. Dilations and transitions of a mother wavelet, $\psi(t)$, are represented as,

$$\psi_{a\tau}(t) = \frac{1}{\sqrt{a}}\psi\left(\frac{t-\tau}{a}\right) \tag{1}$$

where t and τ are the dilation/scaling and translation parameters. For any square-integrable function, $x(t)$, its continuous wavelet transform is,

$$W_{a\tau}\, x(t) = \int x(t)\psi_{a\tau}(t)\,\mathrm{d}t \tag{2}$$

For N number of data points $x(i)$, $i = 1, 2, \ldots, N$, discrete wavelet coefficients W_{jk} at dyadic scales j and displacement k is,

$$\psi_{jk}(i) = 2^{j/2}\psi(2^j i - k) \tag{3}$$

$$W_{jk} = \frac{1}{\sqrt{N}}\sum x(i)\psi_{jk}(i) \tag{4}$$

where $j = 0, 1, \ldots, p$, $k = 1, \ldots, 2^p$ with $p = \log N/\log 2$. A low j implies a fine scale, while a high j indicates a coarse scale.

An original signal can be decomposed into many lower resolution components. Each level of decomposition contains information associated with a scale. A pseudo-frequency can be associated to a given scale [8]. The quality of signal decompositions and reconstruction mainly depends on the choice of the mother wavelet [9]. After decomposition, high-scale and low-frequency components of the signal is called approximations (A), and low-scale and high-frequency components of the signal is called details (D). A very useful parameter that can be calculated from wavelet decomposition is wavelet energy or power. The power P_j in different dyadic scales j is,

$$P_j = \sum_{k=1}^{2^{p-j}} |W_{jk}|^2 (j = 0, 1, \ldots p) \tag{5}$$

In the investigation of flow dynamics in fluidized beds and multi-phase flow using wavelet analysis, the selection of mother wavelets varies considerably from one study to another. The selected wavelet should well represent the characteristics of original signals, and therefore also depends on the type of probe and sampling parameters. In this study, Daubechies wavelet with an order of 6 (DB6) has been chosen for the analysis of experimental data. Daubechies wavelets have a highest number of vanishing moments for a given support width, ensuring that the signal analysis becomes more precise with the higher order of polynomials

used for approximation [8,10,11]. Matlab with wavelet toolbox was used for signal process in this work.

3.2. Statistical and chaos analyses

Average cycle time (ACT) was used to characterize the average time interval of non-periodic pressure fluctuation. ACT is calculated using equation as follows [12,13]:

$$\mathrm{ACT} = \frac{\text{total time}}{(\text{number of crossing with the average})/2} \quad (6)$$

However, ACT from crossing frequency methods normally underestimates the time interval if the time series is very noisy. Alternatively, the dominant cycle time (DCT) [13,14] originated from Hurst [15] was considered for it is not affected by varying sampling frequency of the original time series and linear operations of the original time series.

Chaos analysis was also used to investigate the flow dynamics of the gas–solids fluidized bed. Kolmogorov entropy (K), one of the most useful and frequently used chaos parameters, was used to characterize the chaotic flow behavior. K reflects the information loss rate and predictability into the future, and the definition of K can be found in Grassberger and Procaccia [16]. K was estimated from pressure fluctuation measurements and detail wavelet coefficient using the maximum likelihood method [17] to characterize the multiscale flow behavior. More recent information on statistical, spectral, and chaos analysis of pressure fluctuation can be found elsewhere [18].

4. Results and discussion

Wavelet based denoising methods by Roy et al. [19] was applied to the experimental pressure measurements. In this method, by differentiation of measured time series, contribution due to white noise moves toward the finer scales and this process distributes more energy to finer scales. Scalewise power versus scale (1–14) was first plotted. Thresholding scale level was identified as 2, therefore wavelet coefficients of scales 1 and 2 were set to be zero in the reconstruction of the denoised pressure fluctuation signal. The high frequency components were successfully removed after wavelet denoise.

4.1. Characterization of gas–solids flow behavior from denoised pressure fluctuation

Experimental results showed, as expected, that average pressure decreases with an increase of distance from distributor or a decrease of superficial gas velocity. The reduction in the average pressure was more significant in the bottom part of the bed (h = 6–16 cm), and was attributed to the initial acceleration of some of the particles. The average cycle time was determined from pressure data and results are shown in Fig. 2. ACT varies similarly with operating conditions for glass beads and polyethylene, ACT for glass beads being much higher than that of polyethylene under similar operating conditions. This result suggests that bubbles formed using glass beads are much larger than those for polyethylene powder. Bubble property is greatly affected by particle property, such as particle density, particle diameter, and fluid viscosity. In this work, the density of glass beads is much larger than that of polyethylene particles. Glass beads particles are close to spherical but polyethylene particles are normally non-spherical and porous. This may affect the effective mean particle diameter and particle flow behavior in the fluidized bed. Which greatly affects bubble properties, such as bubble diameter. From published correlations for bubble diameter (e.g., Mori and Wen [20]), there should be larger bubbles for glass beads system compared to polyethylene particle system. This was verified from X-ray fluoroscopy measurements (Fig. 3). Bubbles formed using glass beads were well defined compared to those seen with polyethylene powder [7]. The gas distribution for polyethylene would therefore be more uniform with low ACT, and may enhance the heat and mass transfer in fluidized bed reactors. ACT increases with an increase of U_g, which means large pressure fluctuations, caused by the formation of bubbles with large diameter (Fig. 3), become dominant at higher U_g.

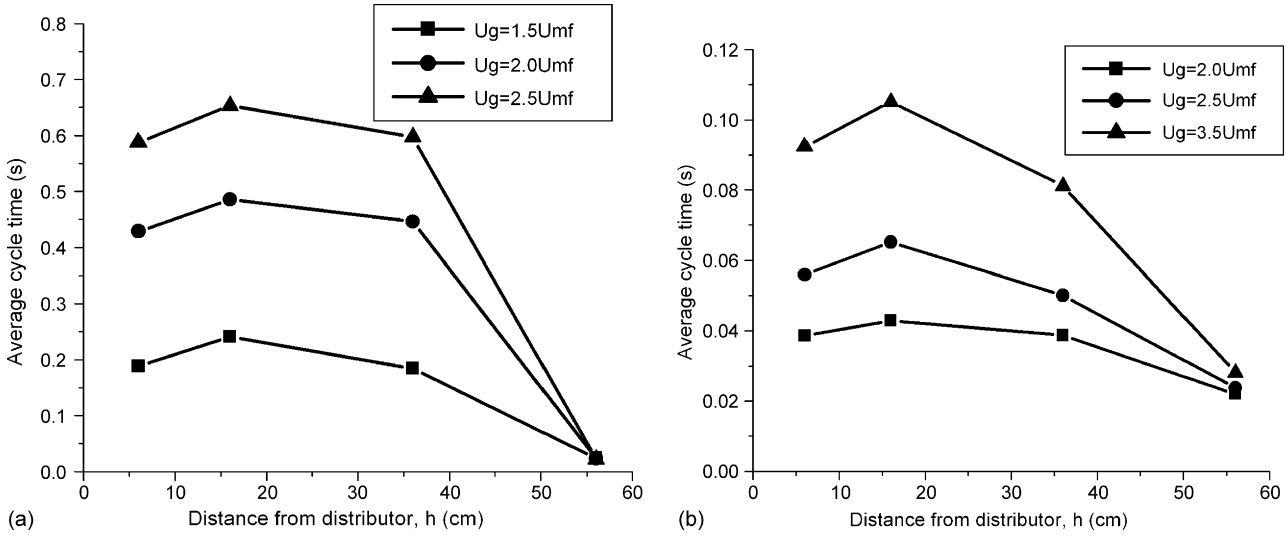

Fig. 2. Average cycle time for (a) glass beads and (b) polyethylene powder from denoised pressure signal.

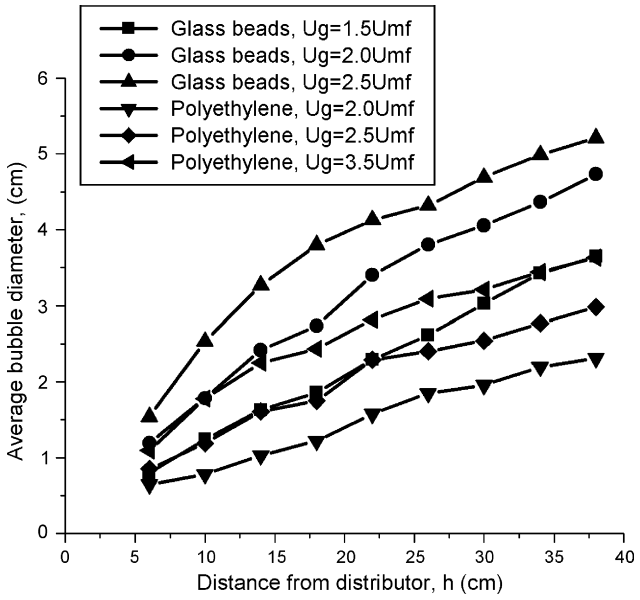

Fig. 3. Average bubble diameter as a function of distance from distributor (from X-ray fluoroscopy experiments).

ACT decreases significantly at $h = 56$ cm, which means that the pressure fluctuations at this position have low amplitude and high frequency. The static bed height is only 40 cm. At $h = 56$ cm, the solids phase is very dilute and the pressure fluctuation is mainly due to gas phase and bubble breakage at the top of the dense bed, therefore the fluctuation is weak and frequent with low ACT. The relatively high value of ACT at bed height around 15 cm is likely due to the coalescence of medium-sized bubbles. As pressure fluctuation mainly reflect the global bubble behavior, the ACT does not change significantly except at $h = 56$ cm. Results presented in Figs. 3–5 suggest that the bubble size steadily increase with the bed height, the number fraction of bubble thus decreasing (Fig. 4) as the bubble velocity remains relatively unaffected by the gas velocity and position in the column. The number of small bubbles formed at lower bed height is likely underestimated because of averaging effects on the overall density [7]. Moreover, overlapping bubbles may have been

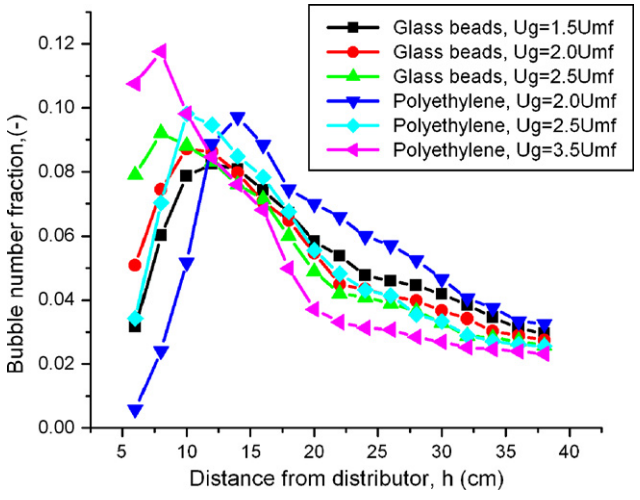

Fig. 4. The distribution of bubbles as a function of distance from distributor.

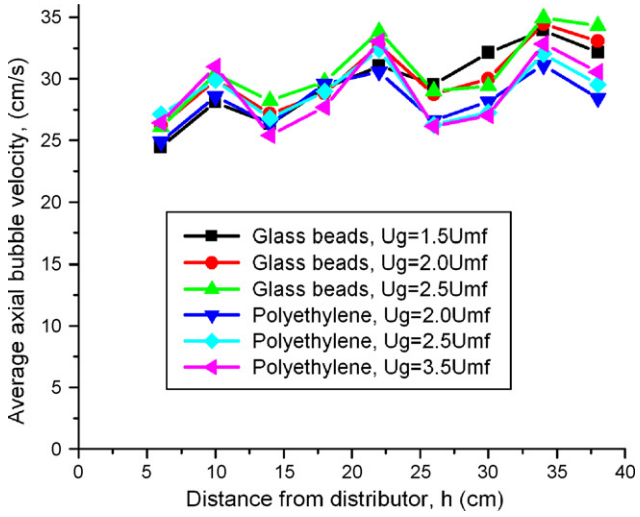

Fig. 5. Average axial bubble rise velocity as a function of distance from distributor (from X-ray fluoroscopy experiments).

detected as single objects. Therefore, the number fraction of small bubble is relatively low at position close to the distributor. Yet, experimental results are very consistent with that presented in the literature and the following question must be considered: is the ACT obtained from pressure signal affected by features other than bubble size and frequency? The reduction in ACT might have been the result of other factors that are known to affect pressure fluctuations such as wave propagation caused by the eruption of bubbles at the bed surface.

Kolmogorov entropy (K) was calculated as shown in Fig. 6. For glass beads, K remains at very low values, compared to polyethylene powder, and is more or less unaffected by changes in U_g. Relatively low K values indicate a less chaotic flow. The results presented in Fig. 6 suggest that the flow structure of glass beads system should be similar once above minimum fluidization velocity. The regular bubbling behavior for glass beads particles causes well-organized flow pattern, which is more likely to be predicted. The high K at $h = 56$ cm is probably due to weak and frequent fluctuations of gas phase and dilute particles, which is very chaotic.

The polyethylene powder bed showed higher K values compared to glass beads, with a strong dependence on both superficial gas velocity and distance from the distributor, suggesting a more chaotic flow pattern for smaller bubbles. K is relatively high in the bottom and upper section of the bed but shows a minimum in the medium section of the bed. Near the distributor, there is relatively large number of small bubbles forming, growing, and coalescing which causes flow behavior very chaotic and less predictable with high K. In the upper section of the bed above the dense bed surface ($h = 56$ cm), weak gas phase fluctuations are dominant and generate relatively high K. The Kolmogorov entropy decreases with an increase in U_g, as high gas velocity introduces large bubble or stronger gas phase fluctuation, which lead to a more regular flow behavior. Therefore, for gas–polyethylene bubbling fluidized bed, flow behavior is more predictable under higher U_g with large bubbles. However, it is expected, under such conditions, that a less chaotic

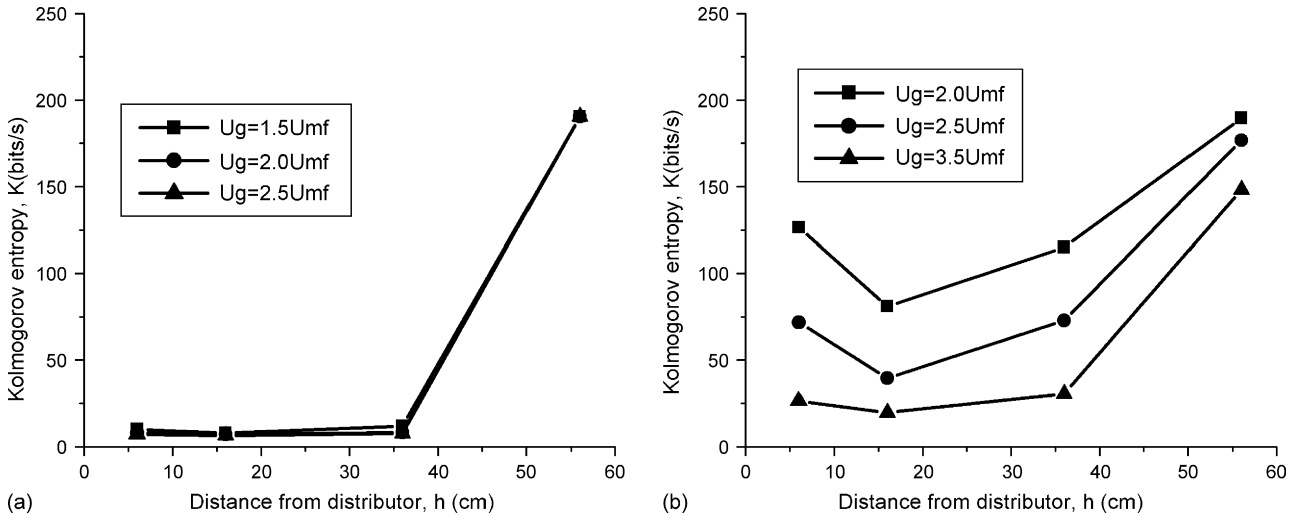

Fig. 6. Kolmogorov entropy for (a) glass beads and (b) polyethylene powder.

flow behavior will lead to less intensive heat and mass transfer phenomena.

4.2. Characterization of multiscale flow behavior using wavelet decomposition

The above analysis results are still general statistical characters over the sampling period. The results reflect flow behavior of all scales. It is necessary to find out what are more local related behavior and the dynamic flow due to different scale. For example, pressure fluctuation caused by medium-sized bubble closed to the pressure port.

Signal series were generally decomposed into approximations and details of different scales. The flow dynamics in the fast fluidized bed systems is discussed at three levels of details [21–22]: micro-scale signals characterizing individual particle movement, meso-scale signals describing bubble and emulsion phases, and macro-scale accounting for the effect of the fluidized bed unit on the system behavior. Each level of information decomposed by wavelet represents information of different frequency band of original signals [23]. Examples of decomposition of pressure fluctuations are shown in Figs. 7 and 8. Pressure signal can be decomposed into higher scales (>6). However, it was difficult to estimate some parameters (e.g. K) with limited

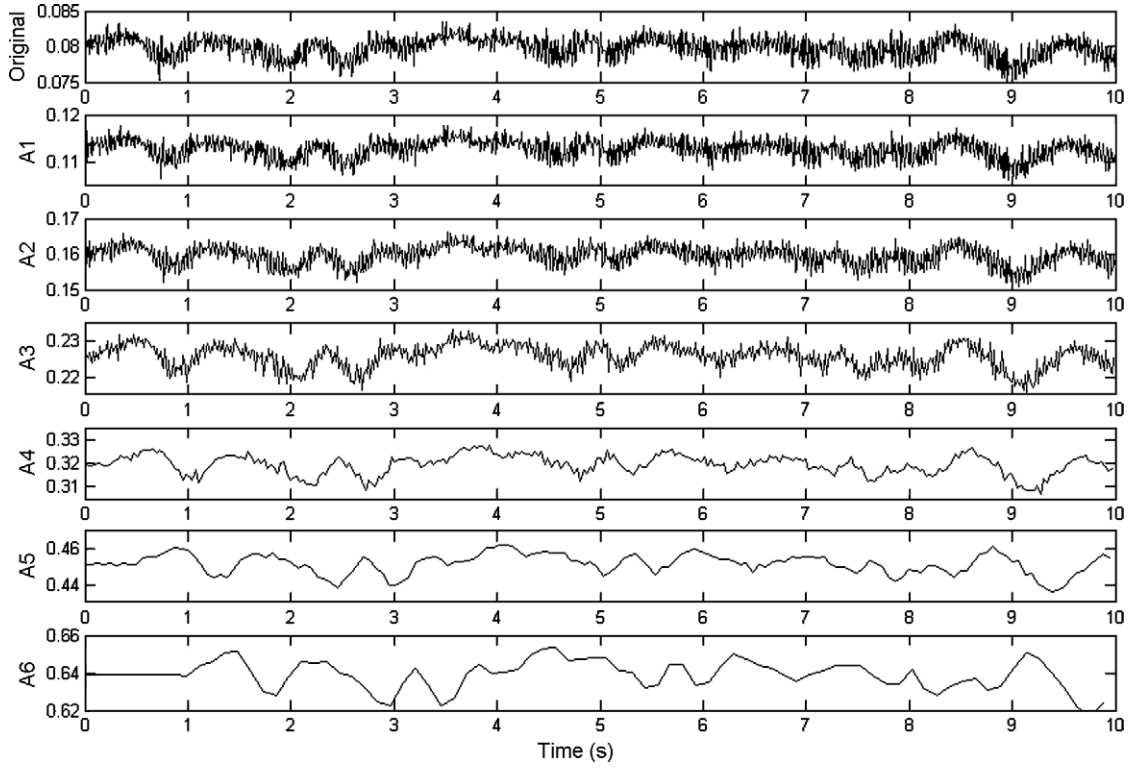

Fig. 7. Original pressure series and approximate coefficients series of scale 1–6 at $U_g = 2U_{mf}$ and $h = 36$ cm for polyethylene powder.

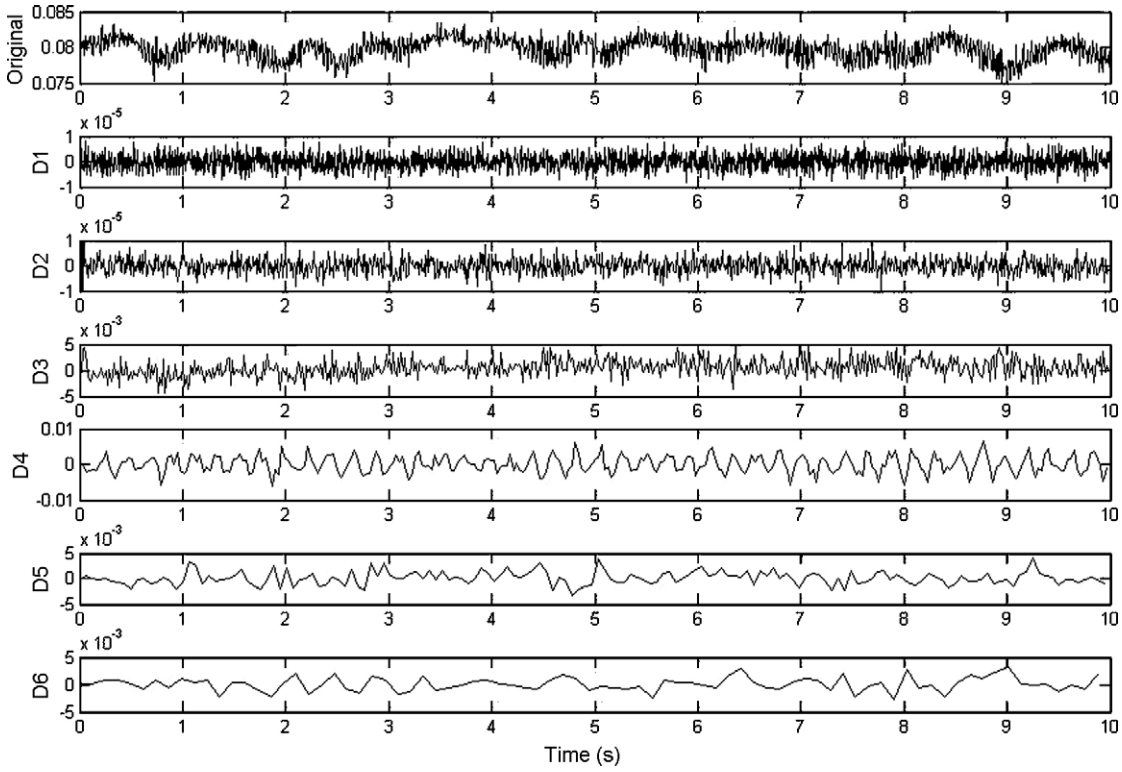

Fig. 8. Original pressure series and detail coefficients series of scale 1–6 at $U_g = 2U_{mf}$ and $h = 36$ cm for polyethylene powder.

data points at very large scales. At very high scale, the decomposed data are very smooth and some useful information was filtered. As such, high scales (>6) were not analyzed in this work.

Figs. 7 and 8 illustrate well the reduction in the high-frequency components with the scale in the approximation and detail series. Fluctuation is very chaotic with mainly high-frequency and low-amplitude components for D1–D3, while there are more relatively large and smooth fluctuations in D4–D6. The approximate series A4–A6 show less small-scale fluctuation and A6 was used for further analysis of global bubbling behavior (macro-scale).

Dominant cycle time and average cycle time were calculated from approximate series at scale 6 (A6) providing information about the global bubbling behavior, as shown in Figs. 9 and 10. ACT of A6 (Fig. 10) is much higher than that from original series due to the clean and smooth nature of large-scale approximate series. In contrast to the trend shown in Fig. 2(a) using the original series for glass beads, ACT and DCT generated from A6 decrease with an increase of U_g at $h < 36$ cm. Most of small fluctuations with high frequency and low amplitude in the original series at lower U_g were removed in A6, the remaining series reflecting the time interval of appearance of large bubbles. A

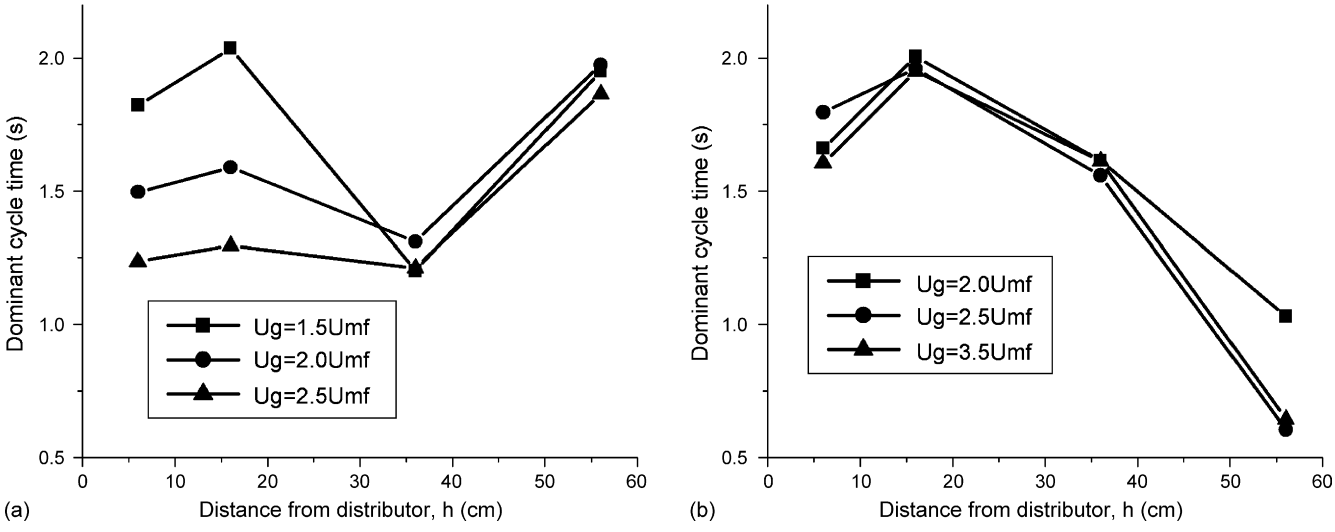

Fig. 9. Dominant cycle time for approximate coefficients of scale 6 (A6) for (a) glass beads and (b) polyethylene powder.

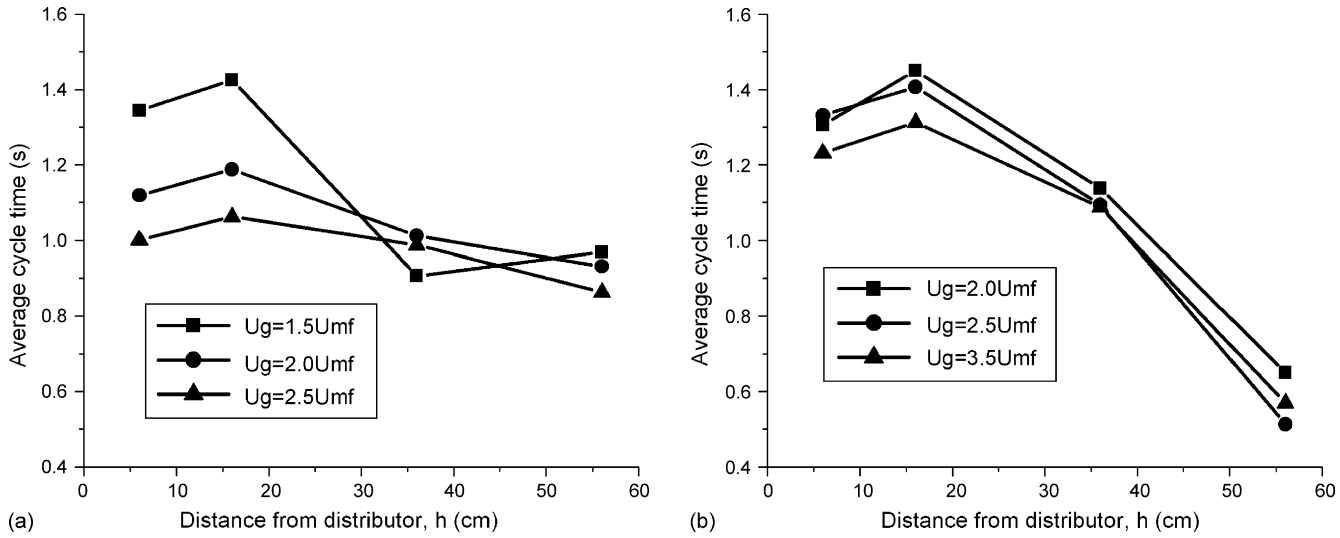

Fig. 10. Average cycle time for approximate coefficients of scale 6 (A6) for (a) glass beads and (b) polyethylene powder.

large ACT indicates the contribution of less frequent and larger bubbles to the original pressure fluctuation. DCT further captures larger scale trends in A6 than ACT, which makes DCT much higher than ACT at $h = 56$ cm. For polyethylene powder, ACT and DCT from A6 vary with bed height and show similar trends. ACT and DCT from A6 do not show important change with U_g, compared to that seen with the original series (Fig. 2b). This suggests that the appearance frequency of large bubbles does not increase significantly with an increase of U_g, which makes for a uniform gas distribution of small bubble in gas-polyethylene fluidized beds. Average axial bubble rise velocity did not vary significantly with bed height and superficial gas velocity for polyethylene powder as verified from X-ray fluoroscopy measurements (Fig. 5).

Wavelet energy from approximate coefficients varies similarly with scale and bed height for both glass beads and polyethylene particles. Fig. 11 shows examples for polyethylene particles for one bed height ($h = 16$ cm) and one scale (A6). Wavelet energy increases with an increase of scale due to the increase of amplitude of most approximate coefficients with scales using DB6 wavelet. Pressure fluctuations at higher positions of the bed were less frequent, therefore wavelet energy decreases with an increase of distance from distributor. Standard deviation (SD) also varies similarly with scale and h for both glass beads and polyethylene particles as shown in Fig. 12 for polyethylene particles. Explanation for the trends should be similar to those for wavelet energy. Higher SD close to distributor at $h = 6$ cm indicates more frequent pressure fluctuations. Similar values of SD at $h = 16$ and $h = 36$ are due to the combination effect of fluctuation of amplitude and frequency. Lower value of SD close to the bed surface indicates weak pressure fluctuations mainly due to gas phase behavior.

In order to further quantify the difference among D1–D6, ACT and K were calculated as shown in Fig. 13. ACT and K of D1–D6 are not significantly affected by changes in the superficial gas velocity U_g, which is likely due to the rela-

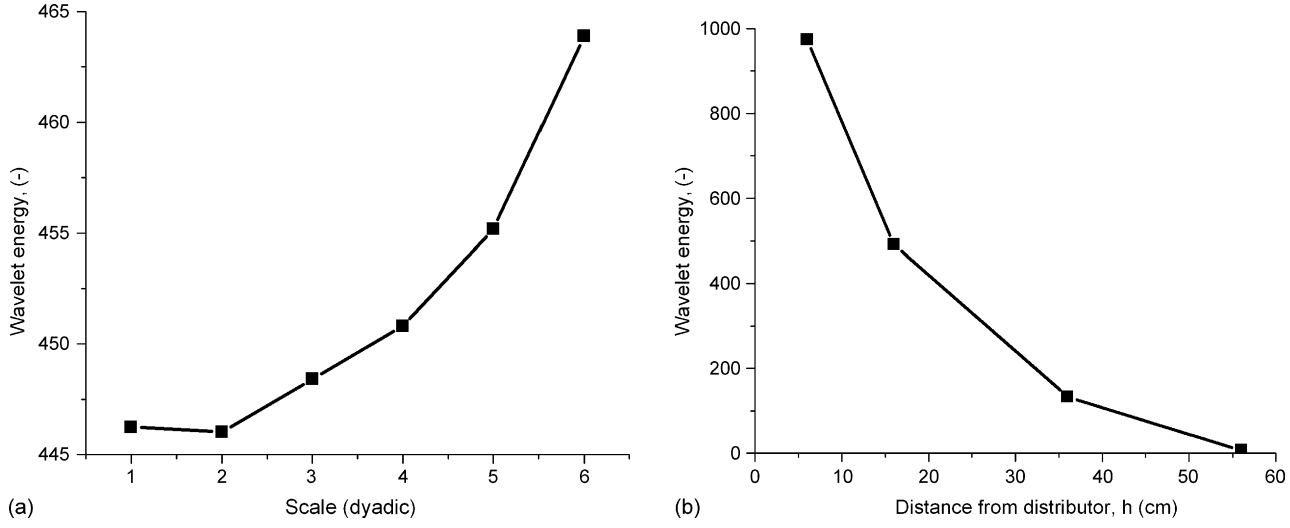

Fig. 11. Wavelet energy estimated from approximate coefficients for polyethylene powder. (a) $U_g = 2U_{mf}$ and $h = 16$ cm; (b) $U_g = 2U_{mf}$ and A6.

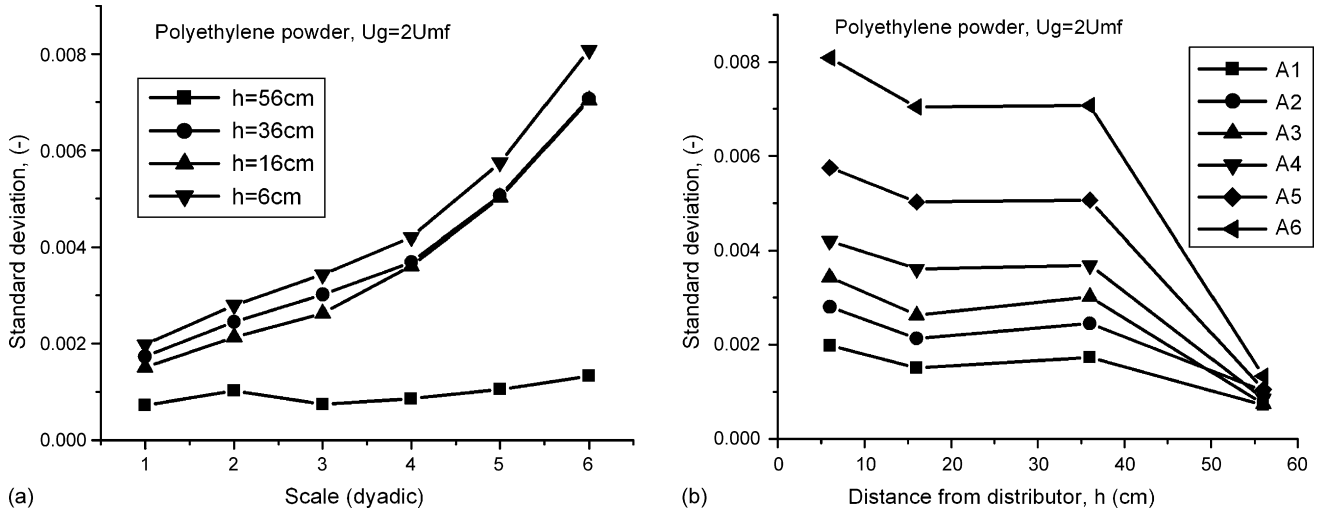

Fig. 12. (a and b) Standard deviation estimated from approximate coefficients for polyethylene powder.

tively small-scale feature of detail series. The values of ACT and K for both glass beads and polyethylene were also similar at comparable operating conditions. Therefore, only the results of polyethylene at one superficial gas velocity are shown in this paper.

ACT increases and K decreases as the scale increases from 1 to 6. This indicates that K is greatly affected by the average cycle time. High-frequency fluctuations with low ACT correspond to high K value, indicating a very chaotic and less predictable bubbling behavior. From the high K value estimated from D1 and D2, the first two scales are likely due to chaotic flow of particles or noise in the bed, which is micro-scale. D3–D6 are likely due to flow behavior of meso-scale bubbles or bubble and dense phase interaction. K and ACT from D3 and D4 change with bed height, indicating local meso-scale bubble flow behavior close to the measurement pressure port. Flow behavior from D5 and D6 is hard to be distinguished from K and ACT for different measurement positions for both glass beads and polyethylene particles. D5 and D6 will be further investigated using wavelet energy and standard deviation.

Wavelet energy and standard deviation estimated from detail coefficients for both glass beads and polyethylene particles are shown in Figs. 14 and 15. Wavelet energy and SD from D1 and D2 are almost the same and close to zero. This confirms that D1 and D2 may be caused by micro-scale behavior of particles or electronic noise. As profile for D3–D6 changes with measurement positions, D3–D6 indicates certain amount of local behavior. Variation of wavelet energy and SD with measurement positions is very significant for D3 and D4, indicating strong local behavior of meso-scale bubbles. D5 is likely caused by the combination of local and global meso-scale bubble behavior. Wavelet energy and standard deviation estimated from D6 varied significantly with measurement positions for glass beads but much less significantly for polyethylene power. This indicated that glass beads are more likely to form large bubbles than polyethylene particles. Large bubbles also caused strong local

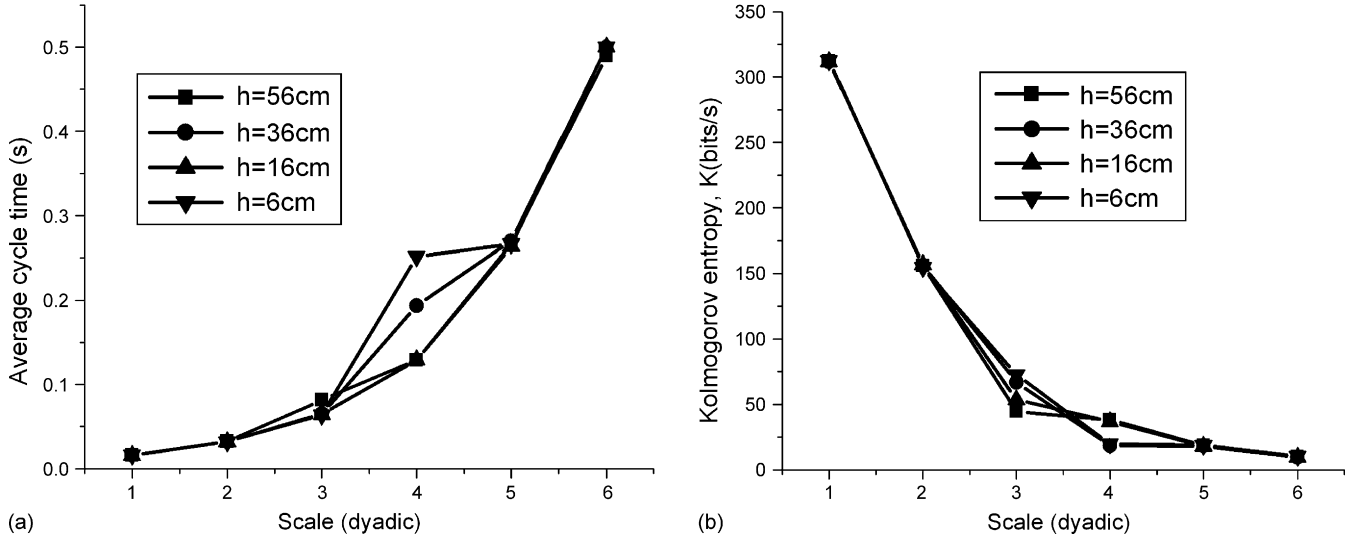

Fig. 13. (a) Average cycle time and (b) Kolmogorov entropy of detail coefficient series (D1–D6) decomposed from denoised pressure fluctuation for polyethylene powder at $U_g = 2U_{mf}$.

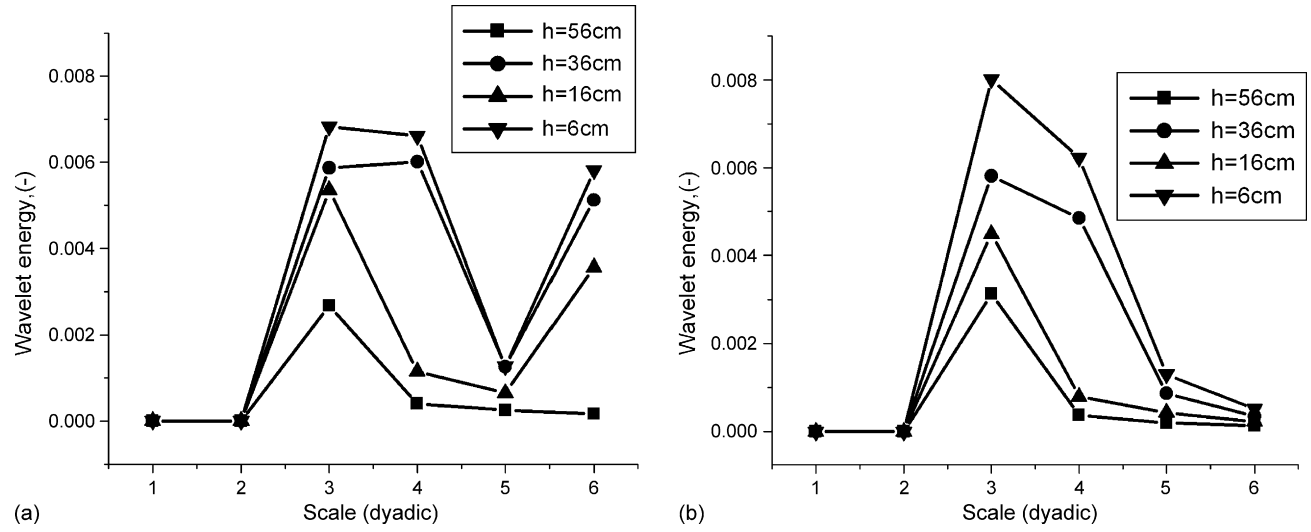

Fig. 14. Wavelet energy estimated from detail coefficient series (D1–D6) decomposed from denoised pressure fluctuation for (a) glass beads and (b) polyethylene powder, at $U_g = 2U_{mf}$.

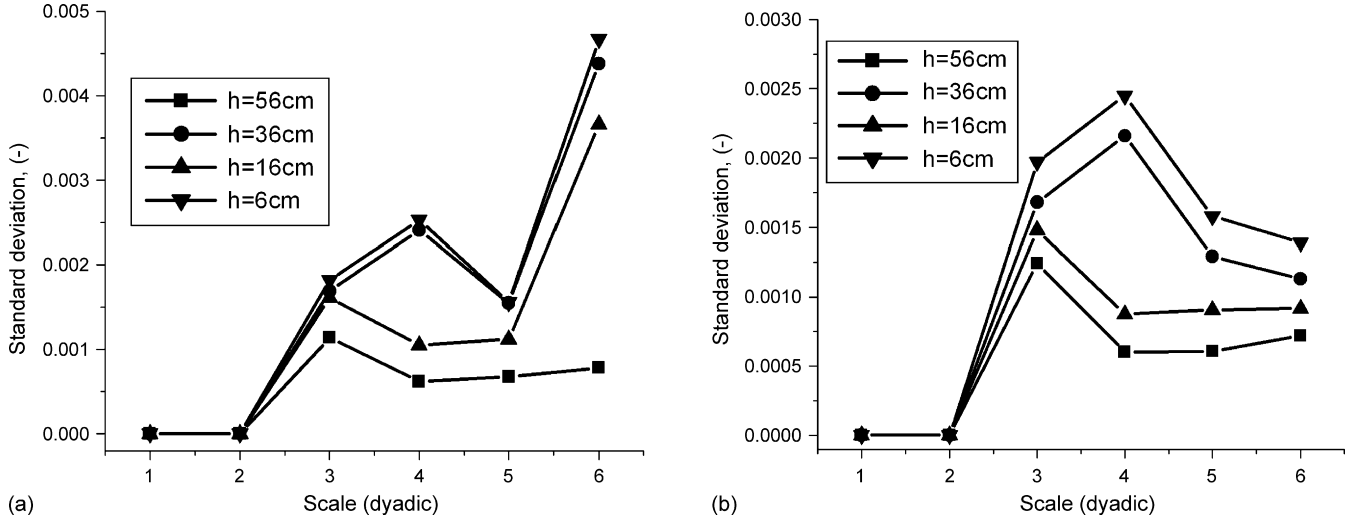

Fig. 15. Standard deviation estimated from detail coefficient series (D1–D6) decomposed from denoised pressure fluctuation for (a) glass beads and (b) polyethylene powder, at $U_g = 2U_{mf}$.

behavior at scale 6 for glass beads. Larger bubble size for glass beads compared to polyethylene under comparable operation conditions was verified from X-ray fluoroscopy measurements (Fig. 5). This indicated that bubble behavior could essentially be captured by pressure fluctuation measurement.

Our results are consistent with those reported by Ellis et al. [10,11]. Further analysis could be performed on the detail coefficient series. The number of peaks (D4 and D5) and peak amplitude may provide information about the bubble frequency [24,25] and bubble diameter [26]. Frequency content of objects could be obtained from wavelet coefficients [1], where smooth coefficients mainly captured the objects of low frequency oscillations (large bubbles) in the pressure signal, and the detail coefficients captured the ones of higher frequency (small bubbles) over the time. Furthermore, wavelet analysis confirms that multi-scale flow behavior is a common phenomenon in gas–solids two-phase flow systems, as reported by Wu et al. [27].

5. Conclusions

Wavelet denoising was effectively used for pretreatment of experimental pressure fluctuation measurements. The similarities and differences of flow dynamics between glass beads and polyethylene powder were identified using ACT and K from denoised pressure series. Multiscale flow behavior was further characterized from wavelet decomposition of denoised time series: global (macro-scale) bubbling flow behavior was represented from A6; D1 and D2 were likely due to micro-scale flow behavior of particles or noise; D3–D4 reflected local meso-scale bubbling behavior; D5–D6 represented meso-scale of large bubbles flow behavior. Glass beads are more likely to form large

bubbles with strong local behavior compared to polyethylene under comparable operation conditions. Similarities and difference of bubbling behavior at different scales for glass beads and polyethylene powder systems from pressure fluctuations were verified from X-ray fluoroscopy measurements. Combination of chaos and wavelet analysis proved to be an effective way to investigate multi-scale behavior in fluidized beds.

Wavelet transforms can provide local dynamics changing with time and detect strange dynamic behavior from pressure measurements. This enable possible monitor and control of flow dynamics in the fluidized bed using pressure measurements.

Acknowledgements

Financial support from the Natural Science and Engineering Research Council of Canada and the Canada Research Chairs Program is gratefully acknowledged.

References

[1] S.H. Park, Y. Kang, S.D. Kim, Wavelet transform analysis of pressure fluctuation signals in a pressurized bubble column, Chem. Eng. Sci. 56 (2001) 6259–6265.
[2] J. van der Schaaf, J.R. van Ommen, F. Takens, J.C. Schouten, C.M. van den Bleek, Similarity between chaos analysis and frequency analysis of pressure fluctuations in fluidized beds, Chem. Eng. Sci. 59 (2004) 1829–1840.
[3] A.A. Kulkarni, J.B. Joshi, V. Ravi Kumar, B.D. Kulkarni, Application of multiresolution analysis for simultaneous measurement of gas and liquid velocities and fractional gas hold-up in bubble column using LDA, Chem. Eng. Sci. 56 (2001) 5037–5048.
[4] Y.G. Chen, Z.P. Tian, Z.Q. Miao, Detection of singularities in the pressure fluctuations of circulating fluidized beds based on wavelet modulus maximum method, Chem. Eng. Sci. 59 (2004) 3569–3575.
[5] H.F. Liu, W.F. Li, Z.H. Dai, Z.H. Yu, The dimension of chaotic dynamical system in wavelet space and its application, Phys. Lett. A 316 (2003) 44–54.
[6] B.R. Bakshi, H. Zhong, P. Jiang, L.-S. Fan, Analysis of flow in gas-liquid bubble columns using multi-resolution methods, Trans. IChemE 73 (1995) 608–614 (Part A).
[7] Z.X. He, Comparison of the behavior of glass-beads and polyethylene resin fluidized beds using X-ray imaging experiments and CFD simulation, M.Sc. Thesis, University of Calgary, Calgary, Canada, 2005.
[8] L.A. Briens, N. Ellis, Hydrodynamics of three-phase fluidized bed systems examined by statistical, fractal, chaos and wavelet analysis methods, Chem. Eng. Sci. 60 (2005) 6094–6106.
[9] M.C. Shou, L.P. Leu, Identification of transition velocities in fluidized beds using wavelet analysis, J. Chem. Eng. Jpn. 38 (6) (2005) 409–421.
[10] N. Ellis, L.A. Briens, J.R. Grace, H.T. Bi, C.J. Lim, Characterization of dynamic behavior in gas-solid turbulent fluidized bed using chaos and wavelet analyses, Chem. Eng. Sci. 96 (2003) 105–116.
[11] N. Ellis, H.T. Bi, C.J. Lim, J.R. Grace, Influence of probe scale and analysis method on measured hydrodynamic properties of gas-fluidized beds, Chem. Eng. Sci. 59 (2004) 1841–1851.
[12] M.L.M. vander Stappen, Chaotic hydrodynamics of fluidized beds, Ph.D. Thesis, Delft University of Technology, Netherlands, 1996.
[13] L.A. Briens, Identification of flow regimes in multiphase reactors by time series analysis, Ph.D. Thesis, The University of Western Ontario, London, Canada, 2000.
[14] E.E. Peters, Fractal Market Analysis: Applying Chaos Theory to Investment and Economics, Wiley, New York, 1994.
[15] H.E. Hurst, Long-term storage capacity of reservoirs, Am. Soc. Civil Engineers 116 (1951) 770–808.
[16] P. Grassberger, I. Procaccia, Characterization of strange attractors, Phys. Rev. Lett. 50 (5) (1983) 346–349.
[17] J.C. Schouten, F. Takens, C.M. van den Bleek, Maximum-likelihood estimation of the entropy of an attractor, Phys. Rev. E 49 (1) (1994) 126–129.
[18] J. Kim, G.U. Han, Effect of agitation on fluidization characteristics of fine particles in a fluidized bed, Powder Technol. 166 (2006) 113–122.
[19] M. Roy, V.R. Kumar, B.D. Kulkarni, J. Sanderson, M. Rhodes, M. vander Stappen, Simple denoising algorithm using wavelet transform, AIChE J. 45 (11) (1999) 2461–2466.
[20] S. Mori, C.Y. Wen, Estimation of bubble diameter in gaseous fluidized bed, AIChE J. 21 (1975) 109–115.
[21] J.Q. Ren, J.H. Li, Wavelet analysis of dynamic behavior in fluidized beds, in: L.S. Fan, T.M. Knowlton (Eds.), Fluidization IX, 1998, pp. 629–636.
[22] J.Q. Ren, Q.M. Mao, J.H. Li, W.G. Lin, Wavelet analysis of dynamic behavior in fluidized beds, Chem. Eng. Sci. 56 (2001) 981–988.
[23] G.B. Zhao, Y.R. Yang, Multi-scale resolution of fluidized-bed pressure fluctuation, AIChE J. 49 (47) (2003) 869–882.
[24] Q.J. Guo, G.X. Yue, J. Werther, Dynamics of pressure fluctuation in a bubbling fluidized bed at high temperature, Ind. Eng. Chem. Res. 41 (2002) 3482–3488.
[25] Q.J. Guo, G.X. Yue, T. Suda, J. Sato, Flow characteristics in a bubbling fluidized bed at elevated temperature, Chem. Eng. Sci. 42 (2003) 439–447.
[26] X.S. Lu, H.Z. Li, Wavelet analysis of pressure fluctuation signals in a bubbling fluidized bed, Chem. Eng. Sci. 75 (1999) 113–119.
[27] B.Y. Wu, L. Briens, J.-X. Zhu, Multi-scale flow behaviors in gas-solids two-phase flow systems, Chem. Eng. Sci. 117 (2006) 187–195.